Coupling of Retinal, Protein, and Water Dynamics in Squid Rhodopsin

Eduardo Jardón-Valadez,[†] Ana-Nicoleta Bondar,[‡§] and Douglas J. Tobias[†§*]
Departments of [†]Chemistry and [‡]Physiology and Biophysics, and [§]Center for Biomembrane Systems, University of California, Irvine, California

ABSTRACT The light-induced isomerization of the retinal from 11-*cis* to all-*trans* triggers changes in the conformation of visual rhodopsins that lead to the formation of the activated state, which is ready to interact with the G protein. To begin to understand how changes in the structure and dynamics of the retinal are transmitted to the protein, we performed molecular dynamics simulations of squid rhodopsin with 11-*cis* and all-*trans* retinal, and with two different force fields for describing the retinal molecule. The results indicate that structural rearrangements in the binding pocket, albeit small, propagate toward the cytoplasmic side of the protein, and affect the dynamics of internal water molecules. The sensitivity of the active-site interactions on the retinal force-field parameters highlights the coupling between the retinal molecule and its immediate protein environment.

INTRODUCTION

The critical physiological functions of G protein-coupled receptors (GPCRs) in cells (1,2) make them important targets for the design of new drugs (3,4). Visual rhodopsin, a member of family A of GPCRs, is an important model system for understanding how GPCRs work. Crystal structures of bovine rhodopsin in the dark- (5–7) and light-adapted states (8–10) provided valuable snapshots of the receptor conformations along the activation path. GPCRs, however, are known as highly dynamic, flexible proteins, that can undergo complex conformational changes in response to ligand binding (4). Rhodopsin transmits a stimulus from its retinal binding pocket up to the cytoplasmic side by a dynamic interplay of interactions involving the retinal, internal water molecules, and the protein (6,11–14). The structure and dynamics of the retinal, as pertains to its coupling to the protein environment, is not clearly understood.

Activation of rhodopsins is triggered by the light-induced ultrafast isomerization of the retinal from the 11-*cis* to the all-*trans* configuration (Fig. S1, *A* and *B*). The recent crystal structure of squid rhodopsin in the dark state (15) revealed structural features that provide clues on how squid rhodopsin may mediate signal transduction. Unlike bovine rhodopsin, which binds a Gt G protein (with the subsequent activation of retinal phosphodiesterase), squid rhodopsin couples to a Gq-type of G protein, leading to the activation of phospholipase C (16,17). The binding of the bovine and squid rhodopsin to different subtypes of G proteins could be due to the different structural features of the cytoplasmic regions of these two proteins: squid rhodopsin has a remarkable extension of transmembrane helices 5 and 6 toward the intracellular side, where the G protein binds (15). Other important structural features that could contribute to a different mechanism of signal transduction in squid rhodopsin are the absence of a strong Schiff base-counterion complex (Fig. S2 *A*), and the presence of a contiguous chain of hydrogen-bonded internal water molecules (IWM) that connect the retinal binding pocket to the cytoplasmic side (15). A role for the IWM in the propagation of conformational change via rearrangements of hydrogen bond (H-bond) networks (15) is supported by the observation that the vibrational fingerprints of at least eight IWM change upon activation of squid rhodopsin (18). From all-atom molecular dynamics (MD) simulations of the squid rhodopsin dark-state conformer in a hydrated lipid bilayer at room temperature, we observed that the interactions of the IWM resolved in the crystal structure are stable on the ~25-ns timescale (19).

The crystal structure of the batho state of bovine rhodopsin solved at cryogenic temperatures (95 K) indicates a distorted all-*trans* retinal geometry, and distinct but rather small changes in the retinal binding pocket relative to the dark state (8). The twisted all-*trans* geometry was stable in optimizations with the approximate density-functional-theory method of self-consistent charge-density functional tight binding (SCC-DFTB) (20,21). A more significant response of the protein to the change in retinal isomerization could be hindered by the cryogenic temperature used to solve the crystal structure. In MD simulations at room temperature starting from 11-*cis* dark-adapted bovine rhodopsin embedded in a hydrated lipid bilayer, conformational changes of the protein could be observed within 30 ns after the geometry of the retinal was set to all-*trans* (22); within ~1 μs of the retinal isomerization, a significant increase in the hydration of the retinal binding site was observed (23). Such a coupling between the structure and dynamics of the retinal and of the protein environment is not surprising, given the tight packing that characterizes the retinal binding pocket in bovine and squid rhodopsin: no fewer than 33 protein amino acids are within 6 Å of the retinal in bovine and squid rhodopsin (Fig. S1, *E* and *F*). This tight packing likely contributes to stabilizing the highly

Submitted April 5, 2010, and accepted for publication June 29, 2010.

*Correspondence: dtobias@uci.edu

Editor: Gregory A. Voth.

0006-3495/10/10/2200/8 $2.00

doi: 10.1016/j.bpj.2010.06.067

twisted geometry of the 11-*cis* retinal in the dark state, and to propagating the structural and dynamic changes from the retinal to the protein upon photoisomerization.

MD simulations allow us to dissect the structural elements that contribute to the coupling between retinal and protein structure and dynamics. Here, we explore the response of the protein to changes in retinal geometry by modeling the all-*trans* retinal state of squid rhodopsin in a hydrated polyunsaturated lipid bilayer. Similar to the observations from MD simulations on bovine rhodopsin (22–24), the results indicate a rapid response of water molecules and of the protein to the change in retinal configuration. The dynamics of the protein and its response to retinal configurational changes are sensitive to the force-field parameters used to model the retinal. This observation confirms the existence of a tight coupling among the retinal, protein, and water molecules toward the onset of conformational changes upon activation.

MATERIALS AND METHODS

MD simulations of squid rhodopsin embedded in a hydrated bilayer of polyunsaturated lipid molecules

For the starting coordinates of protein atoms we used chain B from the crystal structure of squid rhodopsin in the dark state (15). The phospholipid molecule found in the crystal structure was modeled as 1-palmitoyl-2-oleoyl-*sn*-glycero-3-phosphocholine; the palmitoyl tail bonded to C337 was also included as palmitic acid. The side chains of amino acids A356, G357, and E358, which are missing in chain B of the crystal structure (15), were taken from chain A after root mean-square deviation (RMSD) fitting onto chain B. All 29 water molecules present in the crystal structure of chain B were included. The protein, crystallographic water molecules, and the 1-palmitoyl-2-oleoyl-*sn*-glycero-3-phosphocholine lipid were embedded in a bilayer of 1-stearoyl-2-docosahexaenoyl-*sn*-glycero-3-phosphocholine lipids, which provide a realistic representation of the phospholipids found in the rod outer segments (25); the flexibility of polyunsaturated lipids of the rod outer segments assists the conformational changes of rhodopsin upon activation (26). A total of 23,705 solvent water molecules were included, and two chloride ions were added for electroneutrality.

The CHARMM22 (27) and CHARMM27 (28) force-field parameters were used for the protein and lipids, respectively. Water molecules were described by the TIP3P model (29). The force-field parameters used for the retinal atoms are discussed below. The particle-mesh Ewald method (30) was used to calculate the electrostatic interactions with a tolerance of 10^{-6} for the direct part of the Ewald sum, a fourth-order interpolation scheme, and a grid spacing of ~1.0 Å for each box side. A multiple-time-step scheme was used to integrate the equations of motion with time steps of 4 fs for electrostatic forces, 2 fs for short-range nonbonded interactions, and 1 fs for bonded interactions. All bonds lengths involving hydrogen atoms were constrained by using the SHAKE algorithm (31). A Langevin thermostat was used to control the temperature at 300 K (32) and, a Nosé-Hoover-Langevin piston (33,34) to control the pressure at 1 bar. The simulation was performed with the NAMD 2.6 package (32).

In Jardón-Valadez et al. (19) we reported on the structure and dynamics of the dark-state squid rhodopsin from a ~25-ns MD simulation using the setup described here, using the parameters from Nina et al. (35) to describe the retinal, and with weak harmonic constraints of 2 kcal/mol/Å^2 on the retinal heavy atoms. Within 5 ns of MD, the protein structure equilibrated to RMSD values of the C_α atoms of <2 Å. The IWM indicated by the crystal structure (15) remained close to their crystal structure locations, and formed with nearby amino acids a hydrogen-bonded (H-bond) network that was stable during the ~20-ns production segment of the simulation. The equilibrated system of squid rhodopsin in a hydrated polyunsaturated lipid bilayer from our previous study (19) was used as the starting point for all computations reported here.

Modeling of the all-*trans* retinal squid rhodopsin conformer

The three-dimensional structure of the all-*trans* batho state of squid rhodopsin is not known. To explore the changes in protein and IWM dynamics induced by the 11-*cis* to all-*trans* retinal configurational change, we modeled an all-*trans* squid rhodopsin conformer by using structural information for the all-*trans* batho state of bovine rhodopsin (8). The protocol used to derive the all-*trans* squid rhodopsin conformer is described below.

In the first step, we overlapped the crystal structures of the dark-state bovine (6) and squid rhodopsin (15). Retinal interactions in the binding pocket of bovine and squid rhodopsin with conserved residues such as W274, F209, F205, Y190, Y177, and G180, are similar in the two proteins (Fig. S1, *C* and *D*). Because the bovine rhodopsin amino acids G89 and E113 are replaced by N87 and Y111 in squid rhodopsin (15), the retinal Schiff base interactions are different in these proteins. In bovine rhodopsin, the Schiff base is part of an H-bond network involving T94, E113, and a water molecule, whereas the retinal Schiff base of squid rhodopsin does not interact with anionic residues (Fig. S2 *A*).

A comparison of the retinal binding pocket of bovine rhodopsin in the 11-*cis* dark state and all-*trans* batho state reveals very small differences (Fig. S2 *B*; (6,8)). An overlap of the retinal molecule and side chain of K296 from bovine rhodopsin batho-state onto the corresponding atoms of squid rhodopsin dark-state gave an RMSD of 0.68 Å for the heavy atoms. To model an all-*trans* state of squid rhodopsin, we replaced, with the coordinates of the all-*trans* retinal from bovine rhodopsin (8), the coordinates of the 11-*cis* retinal in the equilibrated structure of squid rhodopsin dark state from Jardón-Valadez et al. (19). The closest interaction between the all-*trans* retinal and the squid rhodopsin dark-state protein atoms was between the retinal C_{20} methyl and the hydroxyl group of S187 (2.7 Å).

In the next step, we optimized the geometry of the all-*trans* retinal in the squid rhodopsin dark-state structure by using a combined quantum mechanical/molecular mechanical (QM/MM) approach with SCC-DFTB (21) for the QM region. SCC-DFTB provides a reasonable description of the geometry of the retinal molecule and its interactions with the protein and nearby water molecules (6,36–41). The retinal molecule and the side chain of K305 were described with QM; a hydrogen link atom (42) was placed on C_β of K305. Protein atoms and internal water molecules within 15 Å of Schiff base nitrogen atom were allowed to move during the optimization, but the remaining protein atoms and water molecules were kept fixed. The optimization was performed in 20 steps with harmonic constraints placed on the heavy atoms gradually released from 10.0 kcal/mol/Å^2 to 1.0 kcal/mol/Å^2 in steps of 1.0 kcal/mol/Å^2, and from 1.0 kcal/mol/Å^2 to 0.0 kcal/mol/Å^2 in steps of 0.1 kcal/mol/Å^2. The starting and optimized geometries of the all-*trans* retinal in the squid rhodopsin binding pocket are shown in Fig. S2 *C*. The distance between the C_{20} methyl and the S187 hydroxyl group increased upon geometry optimization by 0.57 Å. Only minor structural rearrangements are observed for the retinal binding pocket groups (Fig. S2 *D*).

Description of the retinal molecule in MD simulations

Ideally, the conjugated polyene system of the retinal molecule would be described with QM. QM methods are, however, impractical for molecular dynamics simulations of retinal proteins in a hydrated lipid membrane for timescales relevant to the issues addressed here. Several sets of retinal force field parameter sets have been derived and used for classical MD

simulations (35,43–45). The retinal parameter sets described in the literature (35,44), hereafter denoted as RP1 and RP2, respectively, are distinguished by the QM methods used to derive the torsional properties of the retinal chain, and by the partial charges of the retinal atoms. RP1 is based on Hartree-Fock and MP2 computations and accounts for the Schiff base-water interactions; RP2 is based on gas-phase B3LYP computations (45–47). The torsional barriers are larger in RP2 than in RP1. For example, the barrier for torsion around the C11=C12 bond is 35.08 kcal/mol in RP2 as compared to 8.75 kcal/mol in RP1.

To assess the sensitivity of the simulation results to the force-field parameters for describing retinal in a protein environment, we performed four independent sets of MD simulations of squid rhodopsin in the 11-*cis* and all-*trans* states using RP1 and RP2 (Table 1). Two additional simulations, corresponding to 11-*cis* and all-*trans* retinal geometries, were performed using RP1 and weak harmonic constraints (2 kcal/mol Å) on the retinal heavy atoms. Each of the six molecular dynamics simulations was prolonged to ~30 ns (Table 1).

Trajectory analysis

To identify the structural elements of the protein that are most sensitive to changes in retinal geometry, we calculated the RMSD for the protein backbone atoms separately for each of the transmembrane helices and the loops. We monitored the time evolution of specific geometric parameters, such as H-bonds, protein-retinal distances, and retinal dihedral angles. As the H-bond criterion we used a cutoff distance of 3.5 Å between the H-bond donor and acceptor atoms, and a direct angle of 40°. Due to protein and IWM dynamics, H-bond pathways connecting different amino acids of the protein break and reform. To quantify the mobility of the IWM around side-chain atoms, we calculated water survival time correlation functions, $n(t)/n(0)$, using a distance cutoff of 3.5 Å between water oxygen atoms and protein donor/acceptor atoms (48). A blocking average method (49) was used to calculate error bars on $n(t)/n(0)$ over the last 18 ns of trajectory for survival times (< 4.5 ns) along consecutive time origins (see Supporting Material). Survival functions were fitted to stretched exponentials,

$$\sim \exp\left[-(t/\tau)^{\beta}\right],$$

with τ and β as adjustable parameters. For $0 < \beta < 1$, residence times were estimated as the average of τ (50),

$$\langle\tau\rangle = (\tau/\beta)\Gamma(1/\beta),$$

where Γ is the Gamma-function, for amino acids D80, S84, S122, W274, S307, and Y315. Residence time errors were calculated by error propagation from errors in the fitting parameters τ and β. Three-dimensional volume maps for the average number density of IWM were calculated over the last 15 ns of trajectory. Density values of 0.1 molecules/Å^3 were traced over grid points in the interhelical space (0.2 Å apart) to construct the isodensity surface, which depicts a three-dimensional histogram of the IWM location. Molecular graphics, visual inspection of trajectories, volume map calculations, and in-house analysis scripts were executed using VMD 1.8.6 (51).

TABLE 1 Summary of simulations performed

Simulation	Retinal geometry	Retinal constraints*	Trajectory Length / ns	RMSD /Å All-Cα atoms	RMSD/Å Retinal + K305	RMSD/Å Protein binding pocket
Sim1†	11-*cis*	On	33.9	1.43	0.79	0.90
Sim2†	11-*cis*	—	32.2	2.86	1.34	1.04
Sim3‡	11-*cis*	—	31.0	1.62	1.55	1.27
Sim4†	all-*trans*	On	31.0	1.48	0.88	0.98
Sim5†	all-*trans*	—	32.3	1.66	2.78	1.30
Sim6‡	all-*trans*	—	29.8	1.58	0.86	1.02

*Harmonic positional constraints of 2 kcal / mol Å^2 were applied to the heavy atoms in Sim1 and Sim4. RMSD averages were calculated for the last 10 ns in each run for all C_α atoms, retinal, and amino-acid heavy atoms within 6 Å of retinal atoms (binding pocket). The initial protein configuration was taken as the reference structure.

†Retinal parameters from Nina et al. (35) (RP1).

‡Retinal torsional barriers from Tajkhorshid et al. (44) (RP2).

RESULTS AND DISCUSSION

Effect of retinal parameters on the structure and dynamics of 11-*cis* squid rhodopsin

As a first step toward exploring the coupling between retinal and protein dynamics, we investigated the sensitivity of the protein structure and dynamics to the description of the retinal geometry and interactions. We prolonged Sim1 to 33.9 ns (Table 1), and performed two independent MD simulations of 11-*cis* dark-adapted squid rhodopsin with RP1 (Sim2) or RP2 (Sim3; Table 1) without positional constraints. We then compared the geometry of the retinal and its binding pocket at the end of Sim1–Sim3 with the starting crystal structure coordinates (Fig. S1, *D* and *F*).

The protein structure remained close to the starting crystal structure in Sim1–Sim3 (Fig. 1 *A*), and most geometric details of the retinal binding pocket are compatible with NMR observations (12). For example, NMR experiments indicate that in the dark state of bovine rhodopsin there are no cross-peaks between retinal atoms C_5, C_6, and C_7 and C_β atom of C167 (W166 in squid rhodopsin). In Sim1–Sim3 we did not observe any contact between retinal and W166 (Fig. 1 *B*). Close interactions were observed between retinal and TM5 amino acids F205 and F209 (Fig. 1 *A*); this is compatible with NMR observations of cross-peaks between F208 and F212 (corresponding to squid rhodopsin F205 and F209, respectively) and retinal atoms C_{16} and C_{17} in the dark state of bovine rhodopsin. Squid rhodopsin TM5-G208 corresponds to bovine rhodopsin H211. According to NMR data (12), H211 interacts closely with the 11-*cis* retinal. Interactions between the squid rhodopsin 11-*cis* retinal and G208 were observed in Sim3, but not in Sim1 and Sim2 (Fig. 1 *B*). This discrepancy between the computations on squid rhodopsin and bovine rhodopsin could be due to differences in the interactions involving His as compared to a Gly amino-acid residue. Except for S275 in Sim1 and Sim3, and A281 in Sim3, TM6 amino acids remained within the cutoff distance of 6 Å (Fig. 1 *B*). Additional TM3 contacts were observed for F118 and S122 in Sim1 and Sim3, respectively, while F113 in Sim3 moved away from retinal (Fig. 1 *B*). The interactions between retinal and TM3 amino acids observed in Sim1–Sim3 are compatible with NMR data on the dark-state of bovine rhodopsin and indicate close interactions between 11-*cis* retinal and amino acids A117, T118, and E122 (12), corresponding, respectively, to squid rhodopsin G115, G116, and F120 (Fig. 1 *B*). The contacts between the

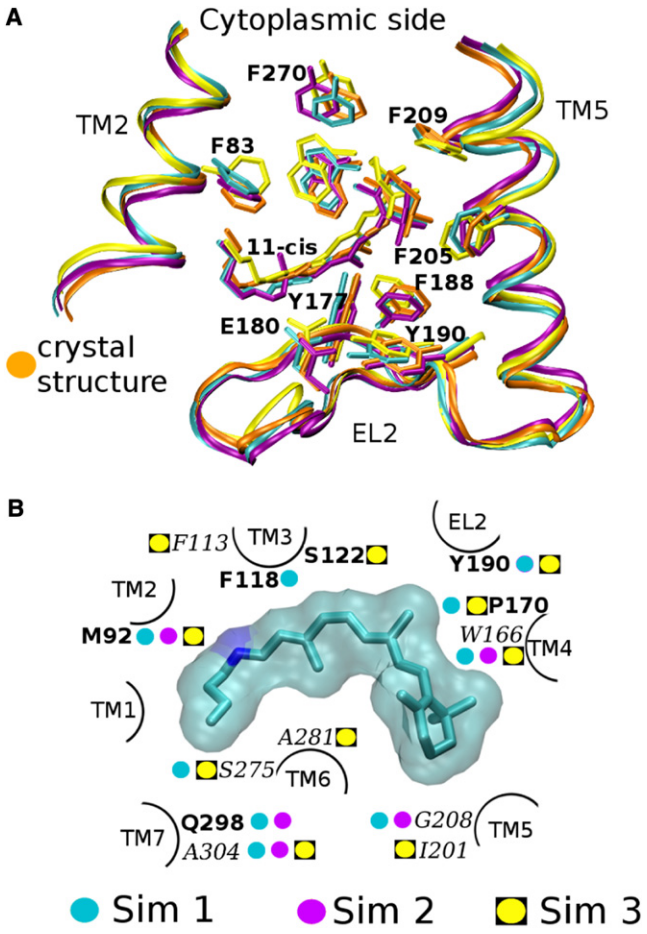

FIGURE 1 Retinal binding pocket in MD simulations of squid rhodopsin in the dark state. (*A*) Overlap of the geometries at the end of Sim1 (*cyan*), Sim2 (*purple*), and Sim3 (*yellow*) on the starting crystal structure (*orange*) (15). For simplicity, only retinal and selected amino-acid side-chain atoms are depicted explicitly. (*B*) Protein amino acids within 6 Å of retinal heavy atoms. Retinal heavy atoms are shown as sticks and transparent surface representation. Bold amino-acid labels represent contacts not present in the crystal structure and found in Sim1 (*cyan circle*), Sim2 (*purple circle*), and/or Sim3 (*yellow circle*); labels in italics represent contacts present in the crystal structure and not found in Sim1 (*cyan circle*), Sim2 (*purple circle*), and/or Sim3 (*yellow circle*). Retinal-protein interactions were identified from average positions over the last 10 ns of simulation. Protein domains for helices TM1-7 and EL2 are indicated to identify amino-acid positions in the protein structure.

extracellular loop 2 (EL2) and the retinal indicated by the crystal structure are well preserved in Sim1–Sim3, including Y190 in Sim 1 and Sim3, as a retinal neighbor (Fig. 1 *B*). Approximately 80% of the retinal contacts observed in the crystal structure of squid rhodopsin are preserved in Sim1–Sim3 (comparison between Fig. S1 *F* and Fig. 1 *B*); conserved amino acids in bovine and squid rhodopsin display equivalent contacts, while differences arise in nonconserved amino acids (Fig. S1, *E* and *F*, and Fig. 1 *B*).

Not surprisingly, given the use of weak harmonic constraints on the retinal heavy atoms, the retinal geometry indicated by the crystal structure was best preserved in Sim1 (Fig. S3). The geometry of the retinal was also well preserved in Sim2, in which most of the dihedral angles remained close to the crystal structure values (Fig. 1 *A* and Fig. S3). An exception are the twists around the single bonds C_{12}-C_{13} and C_{15}-C_{14}, which relaxed significantly relative to the starting crystal structure, respectively, to $-119° \pm 15$ and $44° \pm 21°$ (Fig. S3). In Sim3, retinal tends to become more planar in the C_6-C_7-C_8-C_9-C_{10}-C_{11} segment (Fig. S1 *A*); the twists around the single C_8-C_9 deviate from the crystal structure coordinates to $53° \pm 18°$ (Fig. S3).

The twist of the C_6-C_7 retinal bond defines the orientation of the β-ionone ring relative to the polyene chain. Gas phase QM calculations on the bovine retinal Schiff base show that its stable geometry, in the absence of the protein environment, corresponds to the planar 6-s-*trans* conformation (41). The energetically favored conformation, according to SCC-DFTB calculations, has a C_6-C_7 twist angle of $-166°$; two 6-s-*cis* conformations characterized by C_6-C_7 twist angles of $-28.5°$ and $34.2°$ were found, with energies of, respectively, 0.4 and 0.3 kcal/mol relative to 6-s-*trans* (41). In classical MD simulations on dark-state bovine rhodopsin using RP2 to describe the retinal, two different 6-*s*-*cis* conformers were sampled with twist angles of -60° and 70° (52). The twist of the C_6-C_7 retinal bond in squid rhodopsin, sampled different values of $-60.4° \pm 8.3$ in Sim1, and $8.9° \pm 6.5$ in Sim3; in Sim2 we observed two distinct 6-s-*cis* retinal conformers characterized by twists around the C_6-C_7 bond of $-62° \pm 10$ and at $64° \pm 20$, respectively. The former conformer was predominant (Fig. S5).

The overall deviations of the retinal binding pocket in Sim1–Sim3 calculated relative to the crystal structure indicate that the changes in retinal twists are accompanied by changes in the geometry of nearby protein amino acids. For the binding-site amino acids within 6 Å of retinal heavy atoms (Fig. 1), the RMSD value of 1.77 Å in Sim3, is larger than the values of 0.92 Å and 1.00 Å computed for Sim1 and Sim2, respectively. The larger structural rearrangement of binding pocket amino acids in Sim3 relative to Sim1 and Sim2 is likely due to planarization of the retinal in the C_6–C_{11} segment (Fig. 1 *A*).

All-*trans* retinal model

Changing the retinal configuration from 11-*cis* to all-*trans* causes changes in the dynamics of protein amino acids and water molecules. The differences in dynamics depend on the parameters used to describe the retinal molecule (Fig. 2).

The use of positional constraints in Sim4 maintained the retinal close to the starting QM/MM-optimized all-*trans* geometry (Fig. 2 *A* and Fig. S4). Similar to the observations from Sim1–Sim3, the orientation of the β-ionone ring relative to the retinal polyene chain, and the dynamics of amino

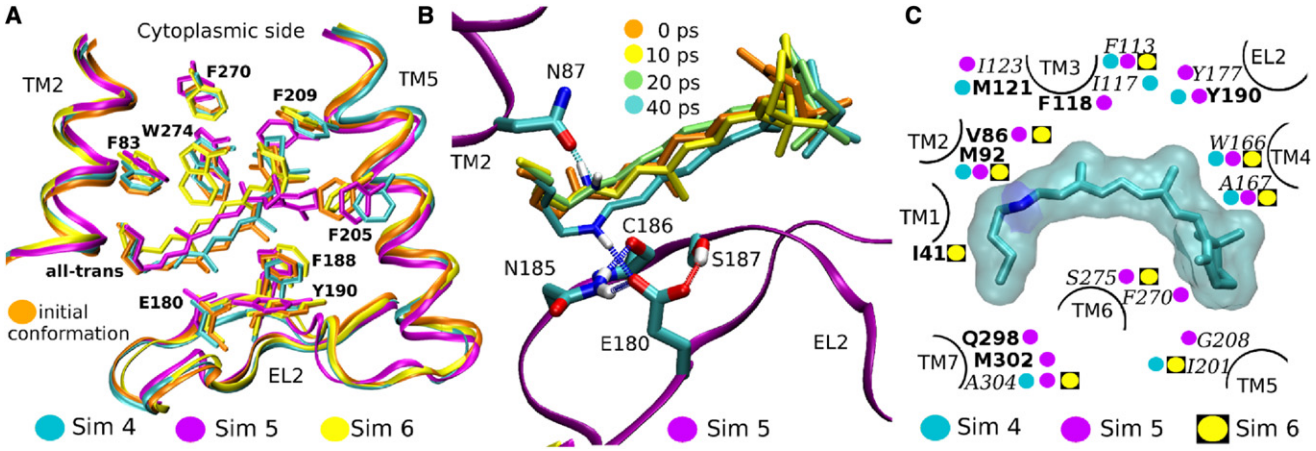

FIGURE 2 Binding pocket of squid rhodopsin in the all-*trans* retinal state. (*A*) Configurations at the end of Sim4 (*cyan circle*), Sim5 (*purple circle*), and/or Sim6 (*yellow*) compared with the starting QM/MM-optimized all-*trans* geometry. The largest deviation of the retinal conformation from the starting configuration was observed in Sim5, where the polyene chain and the β-ionone ring adjust their geometries after reorientation of the protonated Schiff base. (*B*) Snapshots at 0, 10, 20, and 40 ps of Sim5, showing the rotation of the N-H bond (depicted as *blue-white sticks*) from TM2 toward EL2. The rotation switches the H-bond acceptor from N87 to E180, which is the closest anionic residue to the protonated Schiff base. (*Dashed lines*) H-bond interactions. A rotation of the Schiff base N-H bond base has been detected in the metarhodopsin I state of bovine rhodopsin (54). (*C*) Protein amino acids within 6 Å of retinal heavy atoms in the all-*trans* models. Retinal is shown as sticks and transparent surface representations. Amino-acid labels in bold indicate contacts not present in the crystal structure and found in Sim4 (*cyan circle*), Sim5 (*purple circle*), and/or Sim6 (*yellow circle*); labels in italics represent contacts present in the squid rhodopsin crystal structure (15) and not found in Sim1 (*cyan circle*), Sim2 (*purple circle*), and/or Sim3 (*yellow circle*). Retinal-protein interactions were identified from averaged positions over the last 10 ns of simulation. Protein domains for helices TM1–7 and EL2 are shown to indicate amino-acid positions in the protein structure.

acids close to the ring, depend on the parameters used to describe retinal interactions. In Sim4 and Sim5 we detected two 6-s-*cis* conformers characterized by twists of C_6-C_7 of $-49^\circ \pm 8.0$ and $51^\circ \pm 8.7$ in Sim4, and $-48^\circ \pm 10$ and $58^\circ \pm 17$ in Sim5. The conformer with C_6-C_7 negative twist was more predominant in Sim5 than in Sim4 (Fig. S5). Likewise, the absence of positional constraints in Sim5 allows new interactions of the protonated Schiff base (Fig. 2 *C*). As in the 11-*cis* dark-state (Fig. S2 *A*), the QM/MM-optimized all-*trans* Schiff base interacts with N87 (Fig. 2 *B*). Within 40 ps of Sim5, the Schiff base NH bond reorients toward EL2, and H-bonds with E180; E180 also interacts with N185, C186, and S187 (Fig. 2 *B*). The reorientation of the Schiff base NH bond was followed by changes in the orientation of the C_9-CH_3 and C_{13}-CH_3 methyl groups relative to the membrane normal (Fig. S6). After ~10 ns in Sim5, the angle between the C_9-CH_3 and C_{13}-CH_3 bonds and the membrane normal increased, respectively, from 41° and 55° in the starting QM/MM-optimized geometry, to $110^\circ \pm 6.2$ and $130^\circ \pm 19$ (Fig. S6).

To characterize the conformational changes in the retinal binding pocket in Sim4-Sim5, we calculated the RMSD (relative to the QM/MM optimized geometry) of the retinal and K305 heavy atoms, and separately, for amino acids located within 6 Å of the retinal atoms (Table 1). The RMSD values for the retinal and K305 atoms is very small in Sim4 (0.88 Å) and Sim6 (0.86 Å; Table 1). The small deviation of the retinal structure in Sim6 from the starting QM/MM-optimized geometry is explained by the good agreement between the QM method used to derive RP2 (B3LYP;(44)) and the QM method used to describe retinal in the QM/MM optimization (SCC-DFTB; (19,53,54)). The largest deviations of the all-*trans* retinal geometry relative to the starting QM/MM-optimized geometry was observed in Sim5, in which the RMSD for retinal and K305 converged to a value of ~2.8 Å (Table 1). For the amino acids within 6 Å of the retinal heavy atoms, the average RMSD values are small (<1.3 Å; see Table 1) in all three simulations (Sim4–Sim6). The retinal interactions affected by the all-*trans* retinal geometry and parameter sets were specific. For example, in Sim5, the major retinal motion involved in the rotation of the NH bond of the Schiff base (Fig. 2 *B*) allowed contacts between retinal and TM7-M302 not found in the dark state runs (Fig. 1 *B*, Fig. 2 *C*, and Fig. S1 *F*), and the disruption of interactions between retinal with TM1-I123, EL2-Y177, and TM6-F270. Contacts between retinal and residues TM1-F113, TM4-W166 and -A167, and TM7-A304, were lost in Sim4–Sim6 (Fig. 2 *C*). Regardless of the 11-*cis* or all-*trans* retinal geometry, contacts with M92 at TM1 were consistently found in Sim1–Sim6. In contrast, the interactions between retinal and TM4-W166 or TM7-A304 were disrupted in Sim4–Sim6 (Fig. 1 *B* and Fig. 2 *C*). The comparison of contacts between retinal and protein residues, in the 11-*cis* versus all-*trans* geometries, suggest that specific interactions are affected by changes in retinal's geometry, the parameters used to describe retinal, and interactions in the protein environment.

TABLE 2 Residence times for IWM within 3.5 from H-bond donor/acceptor atoms of amino acids connecting W274 with Y315

Amino-acid donor/acceptor	Sim1 $\langle\tau\rangle$/ps	Sim2 $\langle\tau\rangle$/ps	Sim3 $\langle\tau\rangle$/ps	Sim4 $\langle\tau\rangle$/ps	Sim5 $\langle\tau\rangle$/ps	Sim6 $\langle\tau\rangle$/ps
D80 (C=O)	410.4 ± 3.5	413.6 ± 2.8	180.9 ± 2.2	105.1 ± 4.3	215.8 ± 2.0	241.4 ± 9.5
D80(C-O$^-$)	650.1 ± 3.5	204.6 ± 0.8	136 ± 3.9	476.0 ± 3.4	56.6 ± 0.3	447.2 ± 2.7
S84(OH)	74.8 ± 2.3	35.6 ± 2.9	40.5 ± 2.1	95.5 ± 0.6	76.6 ± 0.7	31.3 ± 1.1
S122(OH)	*	23.8 ± 0.4	54.6 ± 0.4	20.5 ± 1.0	13.4 ± 0.7	175.4 ± 0.8
W274(NH)	0.5 ± 0.2	2.8 ± 0.2	4.08 ± 0.08	0.8 ± 0.2	1.2 ± 3.1	4.0 ± 0.2
S307(OH)	57.9 ± 1.5	19.7 ± 0.3	28.0 ± 0.6	9.9 ± 0.4	38.6 ± 0.2	96.7 ± 0.2
Y315(OH)	235.6 ± 9.6	760.4 ± 2.0	413.6 ± 2.8	*	*	232.7 ± 2.9

The average residence times were computed by fitting $n(t)/n(0)$ (representing the probability of finding a molecule at H-bond distance at time t given that it was found at time $t = 0$) to a stretched exponential function (see Supporting Material for details).
*Data not adequately described by a stretched exponential.

Role of the internal water molecules

On the ~30-ns timescale of Sim4–Sim6 the number of IWM remained similar to that in the dark state runs, Sim1–Sim3 (Fig. S7). To investigate the dynamics of the IWM in more detail, we computed the water survival time correlation functions, $n(t)/n(0)$, for the last 18 ns of Sim1–Sim6, for water molecules within 3.5 Å of H-bond donor/acceptor atoms of amino acids D80, S84, S122, S307, W274, and Y315 (Table 2; see section VII in the Supporting Material). Regardless of the retinal geometry, IWM interacting with W274 (Fig. S13 have residence times of approximately picoseconds, whereas IWM close to S84, S122, and S307, have residence times of tens of picoseconds (Table 2). The D80 side chain, located between W274 and Y315, is likely important for mediating H-bond paths between the cytoplasmic side and the retinal binding pocket (see Fig. S13 for examples of H-bond pathways); this side chain remains well hydrated with IWM residence times at the ~100-ps timescale (Table 2). The relatively long residence times of the IWM close to Y315 (Fig. S11; Table 2) suggest that Y315 also contributes to maintaining the H-bond pathways between the binding pocket and the cytoplasmic side (19).

Comparison of the residence times of IWM close to D80 in Sim1–Sim6 (Table 2) suggest that water dynamics is affected by the structure and dynamics of the retinal. In the case of a 11-*cis* retinal geometry, the residence times of IWM close to D80, S84, and S307, are longer when using positional restraints (Sim 1) than without restraints on the retinal atoms (Sim3 and Sim4), which hints at the influence of the retinal dynamics on the IWM dynamics. For the all-*trans* runs, comparing residence times of Sim 4 versus Sim 5 or Sim 6 at D80, S84, S122, and S307, no particular trend is observed; a different IWM dynamics can be related to the retinal geometry that disrupts the protein environment. For instance, the retinal relocation toward TM5 in Sim 5 (Fig. 2, *A* and *B*), where the largest RMSD value for retinal and K305 was found (2.78 Å; Table 1), is reflected in the lower residence times for D80, S84, S122, and S122 in comparison to Sim 4, and for D80, and S307 in comparison to Sim 6 (Table 2).

We further assessed the average dynamics of the IWM by computing the water isodensity surfaces in the interhelical region (Fig. 3). The average location of the IWM depends somewhat on the geometry of retinal. In the all-*trans* geometry, IWM can visit interhelical spaces (grid points in which the density map is calculated) not available when the protein environment hosts 11-*cis* retinal. Because an

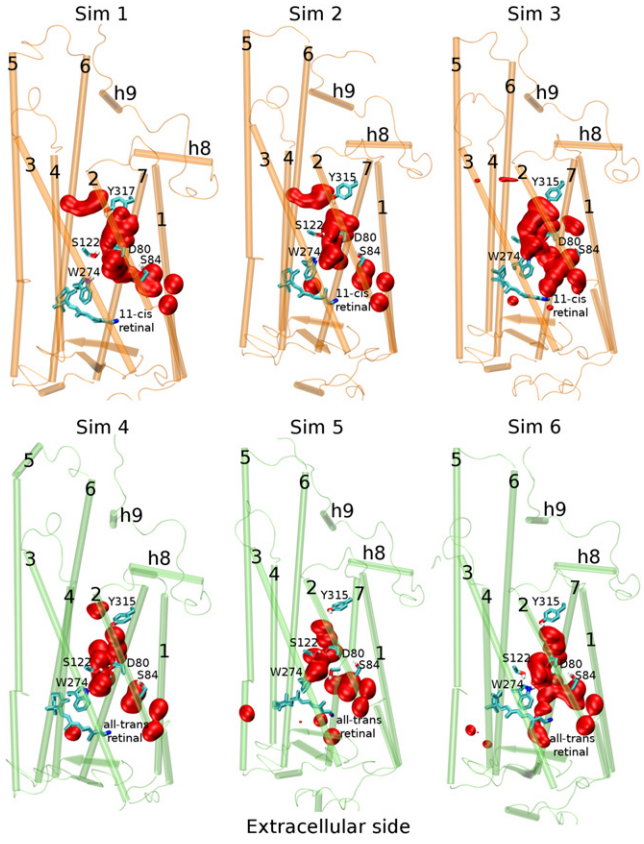

FIGURE 3 Isodensity surfaces (in *red*) of the IWM in the interhelical region. Density values of 0.1 molecules/Å^3 were traced over grid points at 0.2 Å (see text). The calculations were performed using the last 15 ns of each trajectory. Retinal heavy atoms and amino acids D80, S84, S122, W274, and Y315 are depicted as licorice (with carbon atoms, *cyan*; with nitrogen, *light blue*; with oxygen, *red*; and with hydrogen atoms, *light gray*).

average ~6 IWM were found in all runs (Fig. S7), the difference in the isodensity surfaces is due to higher mobility of the IWM over the time interval during which the surfaces were computed, rather than a decrease in the amount of water.

The shortest H-bond path from the Y315 hydroxyl to the indole nitrogen of W274 consists of 4–8 H-bond donor/acceptor partners in the 11-*cis* simulations (Sim1–Sim3; Fig. S12). The most probable H-bond path from Y315 to W274 consisted of seven H-bond partners: D80, S307, and the crystallographic water molecules wat1–wat5 (Fig. S12). In the all-*trans* simulations (Sim4–Sim6), we find that Y315 and W274 are connected by 5–9 H-bond partners (Fig. S13). Compared to the 11-*cis* simulations, the increased dynamics of the IWM in the all-*trans* retinal simulations enhances the likelihood of forming H-bond connections. Within 10 ns of Sim6, wat2, initially located in the interhelical region, exchanged with a bulk water molecule from the cytoplasmic side (bulk-water in Fig. S12); bulk-water remained H-bonded to Y315.

CONCLUSIONS

The MD simulations of the 11-*cis* dark state squid rhodopsin and all-*trans* models indicate that the protein environment is sensitive to the retinal geometry and to the interactions among retinal, protein amino acids, and water molecules. The simulations in which the geometry of the 11-*cis* retinal is maintained close to the starting crystal structure coordinates by using weak harmonic constraints on the retinal heavy atoms preserves well the protein structure and the location of water molecules indicated in the crystal structure (17). In the absence of the harmonic constraints on the retinal heavy atoms, and regardless of the parameter set used to describe the retinal, changes in the twisting of the C_6-C_7, C_{12}-C_{13}, and C_{14}-C_{15} bonds lead to deviations from the geometry of the 11-*cis* retinal indicated by the crystal structure. We observed two different 6-s-*cis* conformations of the β-ionone ring when using RP1 to describe retinal; with RP2, the β-ionone ring became coplanar with the polyene chain. With both RP1 and RP2, relative to the 11-*cis* state the all-*trans* models show subtle but significant changes of the geometry and dynamics of specific protein amino acids. The dependence on the parameters used to describe the retinal on the geometry of the protein (Table 1) and the dynamics of IWM (Table 2) underscores the strong coupling between retinal and its protein and water environment, and points to the need for additional studies that account for how the parameters used could influence the results of retinal protein simulations.

Disruption of interactions between retinal and W166, A167, and A304, and a distinct dynamics of IWM in the all-*trans* model, are associated with stabilization of the H-bonded path that connects the retinal binding pocket to the cytoplasmic side. This enhanced connectivity could contribute to the relay of structural perturbation upon retinal isomerization. The observations here that the dynamics of IWM and the water-mediated interhelical H bonds depend upon the structure and dynamics of the retinal, support the initial proposal of a role of the IWM in signal propagation by squid rhodopsin (15,18), and also highlights the importance of accounting for IWM dynamics in discussing mechanisms of GPCR activation.

SUPPORTING MATERIAL

Thirteen figures and four equations are available at http://www.biophysj.org/biophysj/supplemental/S0006-3495(10)00837-4.

The authors are grateful to Profs. Midori Murakami and Tsutomu Kouyama for valuable discussions. E.J.-V. is indebted to J. Alfredo Freites for developing valuable tools for the analysis of MD trajectories.

This research was supported in part by the National Science Foundation through TeraGrid resources provided by the Texas Advanced Computing Center (grant No. CHE-0750175 to D.J.T.). E.J.-V. is supported by a UC MEXUS-CONACyT postdoctoral fellowship. A.-N.B. is supported by the National Institutes of Health (grants No. GM74637 and No. GM68002).

REFERENCES

1. Kristiansen, K. 2004. Molecular mechanisms of ligand binding, signaling, and regulation within the superfamily of G-protein-coupled receptors: molecular modeling and mutagenesis approaches to receptor structure and function. *Pharmacol. Ther.* 103:21–80.
2. Schöneberg, T., A. Schulz, …, K. Sangkuhl. 2004. Mutant G-protein-coupled receptors as a cause of human diseases. *Pharmacol. Ther.* 104:173–206.
3. Klabunde, T., and G. Hessler. 2002. Drug design strategies for targeting G-protein-coupled receptors. *ChemBioChem.* 3:928–944.
4. Kobilka, B., and G. F. X. Schertler. 2008. New G-protein-coupled receptor crystal structures: insights and limitations. *Trends Pharmacol. Sci.* 29:79–83.
5. Li, J., P. C. Edwards, …, G. F. Schertler. 2004. Structure of bovine rhodopsin in a trigonal crystal form. *J. Mol. Biol.* 343:1409–1438.
6. Okada, T., M. Sugihara, …, V. Buss. 2004. The retinal conformation and its environment in rhodopsin in light of a new 2.2 Å crystal structure. *J. Mol. Biol.* 342:571–583.
7. Palczewski, K., T. Kumasaka, …, M. Miyano. 2000. Crystal structure of rhodopsin: a G protein-coupled receptor. *Science.* 289:739–745.
8. Nakamichi, H., and T. Okada. 2006. Crystallographic analysis of primary visual photochemistry. *Angew. Chem. Int. Ed. Engl.* 45:4270–4273.
9. Ruprecht, J. J., T. Mielke, …, G. F. Schertler. 2004. Electron crystallography reveals the structure of metarhodopsin I. *EMBO J.* 23:3609–3620.
10. Salom, D., D. T. Lodowski, …, K. Palczewski. 2006. Crystal structure of a photoactivated deprotonated intermediate of rhodopsin. *Proc. Natl. Acad. Sci. USA.* 103:16123–16128.
11. Vogel, R., M. Mahalingam, …, T. P. Sakmar. 2008. Functional role of the "ionic lock"—an interhelical hydrogen-bond network in family A heptahelical receptors. *J. Mol. Biol.* 380:648–655.
12. Ahuja, S., E. Crocker, …, S. O. Smith. 2009. Location of the retinal chromophore in the activated state of rhodopsin. *J. Biol. Chem.* 284:10190–10201.
13. Mahalingam, M., K. Martínez-Mayorga, …, R. Vogel. 2008. Two protonation switches control rhodopsin activation in membranes. *Proc. Natl. Acad. Sci. USA.* 105:17795–17800.

14. Okada, T., Y. Fujiyoshi, …, Y. Shichida. 2002. Functional role of internal water molecules in rhodopsin revealed by x-ray crystallography. *Proc. Natl. Acad. Sci. USA*. 99:5982–5987.

15. Murakami, M., and T. Kouyama. 2008. Crystal structure of squid rhodopsin. *Nature.* 453:363–367.

16. Terakita, A., T. Yamashita, …, Y. Shichida. 1998. Selective activation of G-protein subtypes by vertebrate and invertebrate rhodopsins. *FEBS Lett.* 439:110–114.

17. Simon, M. I., M. P. Strathmann, and N. Gautam. 1991. Diversity of G proteins in signal transduction. *Science.* 252:802–808.

18. Ota, T., Y. Furutani, …, H. Kandori. 2006. Structural changes in the Schiff base region of squid rhodopsin upon photoisomerization studied by low-temperature FTIR spectroscopy. *Biochemistry.* 45:2845–2851.

19. Jardón-Valadez, E., A.-N. Bondar, and D. J. Tobias. 2009. Dynamics of the internal water molecules in squid rhodopsin. *Biophys. J.* 96:2572–2576.

20. Schreiber, M., M. Sugihara, …, V. Buss. 2006. Quantum mechanical model of bathorhodopsin. *Angew. Chem. Int. Ed.* 45:4274–4277.

21. Elstner, M., D. Porezaq, …, G. Seifert. 1998. Self-consistent-charge density-functional tight-binding method for simulations of complex material properties. *Phys. Rev. B.* 58:7260–7268.

22. Crozier, P. S., M. J. Stevens, and T. B. Woolf. 2007. How a small change in retinal leads to G-protein activation: initial events suggested by molecular dynamics calculations. *Proteins.* 66:559–574.

23. Grossfield, A., M. C. Pitman, …, K. Gawrisch. 2008. Internal hydration increases during activation of the G-protein-coupled receptor rhodopsin. *J. Mol. Biol.* 381:478–486.

24. Saam, J., E. Tajkhorshid, …, K. Schulten. 2002. Molecular dynamics investigation of primary photoinduced events in the activation of rhodopsin. *Biophys. J.* 83:3097–3112.

25. Albert, A. D., J. E. Young, and Z. Paw. 1998. Phospholipid fatty acyl spatial distribution in bovine rod outer segment disk membranes. *Biochim. Biophys. Acta.* 1368:52–60.

26. Gawrish, K., and O. Soubias. 2008. Structure and dynamics of polyunsaturated hydrocarbon chains in lipid bilayers-significance for GPCR function. *Chem. Phys. Lipids.* 153:64–75.

27. MacKerell, Jr., A. D., D. Bashford, …, M. Karplus. 1998. All-atom empirical potential for molecular modeling and dynamics studies of proteins. *J. Phys. Chem. B.* 102:3586–3616.

28. Feller, S. E., K. Gawrisch, and A. D. MacKerell, Jr. 2002. Polyunsaturated fatty acids in lipid bilayers: intrinsic and environmental contributions to their unique physical properties. *J. Am. Chem. Soc.* 124:318–326.

29. Jorgensen, W. L., J. Chandrasekhar, …, M. L. Klein. 1983. Comparison of simple potential functions for simulating liquid water. *J. Chem. Phys.* 79:926–935.

30. Darden, T., D. York, and L. Pedersen. 1993. Particle mesh Ewald: an $N\bullet\log(N)$ method for Ewald sums in large systems. *J. Chem. Phys.* 98:10089–10092.

31. Ryckaert, J.-P., G. Ciccotti, and H. J. C. Berendsen. 1977. Numerical integration of the Cartesian equations of motion of a system with constraints: molecular dynamics of *n*-alkanes. *J. Comput. Phys.* 23:327–341.

32. Phillips, J. C., R. Braun, …, K. Schulten. 2005. Scalable molecular dynamics with NAMD. *J. Comput. Chem.* 26:1781–1802.

33. Martyna, G. J., D. J. Tobias, and M. K. Klein. 1994. Constant pressure molecular dynamics algorithms. *J. Chem. Phys.* 101:4177–4189.

34. Feller, S. E., Y. Zhang, …, B. R. Brooks. 1995. Constant pressure molecular dynamics simulation: the Langevin piston method. *J. Chem. Phys.* 103:4613–4621.

35. Nina, M., B. Roux, and J. C. Smith. 1995. Functional interactions in bacteriorhodopsin: a theoretical analysis of retinal hydrogen bonding with water. *Biophys. J.* 68:25–39.

36. Elstner, M. 2006. The SCC-DFTB method and its application to biological systems. *Theor. Chem. Acc.* 116:316–325.

37. Bondar, A.-N., J. C. Smith, and M. Elstner. 2010. Mechanism of a proton pump analyzed with computer simulations. *Theor. Chem. Acc.* 125:353–363.

38. Sugihara, M., J. Hufen, and V. Buss. 2006. Origin and consequences of steric strain in the rhodopsin binding pocket. *Biochemistry.* 45: 801–810.

39. Sigihara, M., V. Buss, and J. Hufen. 2004. The nature of the complex counterion of the chromophore in rhodopsin. *J. Phys. Chem.* 108:3672–3680.

40. Bondar, A.-N., J. Baudry, …, J. C. Smith. 2008. Key role of active-site water molecules in bacteriorhodopsin proton-transfer reactions. *J. Phys. Chem. B.* 112:14729–14741.

41. Sugihara, M., V. Buss, …, T. Frauenheim. 2002. 11-*cis*-retinal protonated Schiff base: influence of the protein environment on the geometry of the rhodopsin chromophore. *Biochemistry.* 41:15259–15266.

42. Field, M. J., P. A. Bash, and M. Karplus. 1990. A combined quantum mechanical and molecular mechanical potential for molecular dynamics simulations. *J. Comput. Chem.* 11:700–733.

43. Lamaître, V., P. Yeagle, and A. Watts. 2005. Molecular dynamics simulation of retinal in rhodopsin: from the dark-adapted state towards luminorhodopsin. *Biochemistry.* 44:12667–12680.

44. Tajkhorshid, E., J. Baudry, …, S. Suhai. 2000. Molecular dynamics study of the nature and origin of retinal's twisted structure in bacteriorhodopsin. *Biophys. J.* 78:683–693.

45. Tajkhorshid, E. B. P., and S. Suhai. 1999. Role of isomerization barrier in the pK_a control of the retinal Schiff base: a density functional study. *J. Phys. Chem. B.* 103:4518–4527.

46. Tajkhorshid, E., and S. Suhai. 1999. The effect of the protein environment on the structure and charge distribution of the retinal Schiff base in bacteriorhodopsin. *Theor. Chem. Acc.* 101:180–185.

47. Paisz, B., E. Tarjkhorshid, and S. Suhai. 1999. Electronic effect on the ground-state rotational barrier of polyene Schiff bases: a molecular orbital study. *J. Phys. Chem. B.* 103:5388–5395.

48. Impey, R. W., P. A. Madden, and I. R. McDonald. 1983. Hydration and mobility of ions in solution. *J. Phys. Chem.* 87:5071–5083.

49. Flyvbjerg, H., and H. G. Petersen. 1989. Error estimates on averages of correlated data. *J. Chem. Phys.* 91:461–466.

50. Freites, J. A., D. J. Tobias, …, S. H. White. 2005. Interface connections of a transmembrane voltage sensor. *Proc. Natl. Acad. Sci. USA.* 102:15059–15064.

51. Humphrey, W., A. Dalke, and K. Schulten. 1996. VMD: visual molecular dynamics. *J. Mol. Graph.* 14:33–38, 27–28.

52. Lau, P.-W., A. Grossfield, …, M. F. Brown. 2007. Dynamic structure of retinylidene ligand of rhodopsin probed by molecular simulations. *J. Mol. Biol.* 372:906–917.

53. Zhou, H., E. Tarjkhorshid, …, M. Elstner. 2002. Performance of the AM1, PM3, and SCC-DFTB methods in the study of conjugated Schiff base molecules. *Chem. Phys.* 277:91–103.

54. Brown, M. F., K. Martínez-Mayorga, …, A. V. Struts. 2009. Retinal conformation and dynamics in activation of rhodopsin illuminated by solid-state ^{2}H NMR spectroscopy. *Photochem. Photobiol.* 85:442–453.

55. Reference deleted in proof.